Myosin 1a Regulates Osteoblast Differentiation Independent of Intestinal Calcium Transport

Scott Munson,[1] Yongmei Wang,[1] Wenhan Chang,[1] and Daniel D. Bikle[1]

[1]*Department of Medicine and Endocrine Research Unit, Veterans Affairs Medical Center and University of California San Francisco, San Francisco, California 94158*

ORCiD numbers: 0000-0002-1040-475X (D. D. Bikle).

Myosin 1A (Myo1a) is a mechanoenzyme previously thought to be located exclusively in the intestinal epithelium. It is the principle calmodulin-binding protein of the brush border. Based on earlier studies in chickens, we hypothesized that Myo1a facilitates calcium transport across the brush border membrane of the intestinal epithelium, perhaps in association with the calcium channel Trpv6. Working with C2Bbe1 cells, a human intestinal epithelial cell line, we observed that overexpression of Myo1a increased, whereas the antisense construct blocked calcium transport. To further test this hypothesis, we examined mice in which either or both *Myo1a* and *Trpv6* had been deleted. Although the *Trpv6*-null mice had decreased intestinal calcium transport, the *Myo1a*-null mouse did not, disproving our original hypothesis, at least in mice. Expecting that a reduction in intestinal calcium transport would result in decreased bone, we examined the skeletons of these mice. To our surprise, we found no decrease in bone in the *Trpv6*-null mouse, but a substantial decrease in the *Myo1a*-null mouse. Double deletions were comparable to the *Myo1a* null. Moreover, Myo1a but not Trpv6 was expressed in osteoblasts. *In vitro*, the bone marrow stromal cells from the *Myo1a*-null mice showed normal numbers of colony-forming units but marked decrements in the formation of alkaline phosphatase–positive colonies and mineralized nodules. We conclude that Myo1a regulates osteoblast differentiation independent of its role, if any, in intestinal calcium transport, whereas Trpv6 functions primarily to promote intestinal calcium transport with little influence in osteoblast function.

Freeform/Key Words: intestine, bone, myosin 1A, TRPV6, 1,25 dihydroxyvitamin D, calcium

Intestinal calcium transport occurs by both the paracellular and transcellular routes (review in Hoenderop *et al.* [1]). The transcellular route is the most regulated. The transcellular route is comprised of three major processes: 1) calcium entry into the cell across the brush border membrane down a steep electrochemical gradient through highly calcium-selective channels, Trpv6 in particular; 2) transport through the cytosol mediated by calbindins CaBP9k (mammals) or CaBP28k (avian); and 3) removal by an active calcium pump, members of the PMCA family, at the basolateral membrane. 1,25 dihydroxyvitamin D [1,25$(OH)_2$D] is the major regulatory hormone stimulating intestinal calcium transport. 1,25$(OH)_2$D induces the brush border membrane calcium channel Trpv6 (previously known as ECAC2 or CaT1), induces calbindin either 28k or 9k depending on species, and induces PMCA1b, the major PMCA isoform in the intestine. The induction of Trpv6 by 1,25$(OH)_2$D is faster than that of

Abbreviations: 1,25 $(OH)_2$D, 1,25 dihydroxyvitamin D; μCT, micro-CT; AP, alkaline phosphatase; BMSC, bone marrow stromal cell; BS, bone surface; BV, bone volume; CaM, calmodulin; CFU, colony-forming unit; CPC, cetylpyridinium chloride; DKO, double-knockout; FCS, fetal calf serum; GFP, green fluorescent protein; KO, knockout; Myo1a, myosin 1A; OCN, osteocalcin; QPCR, quantitative polymerase chain reaction; TRAP, tartrate-resistant acid phosphatase; TV, tissue volume; WT, wild-type.

Received 6 May 2019
Accepted 6 August 2019
First Published Online 12 August 2019

ISSN 2472-1972
November 2019 | Vol. 3, Iss. 11
doi: 10.1210/js.2019-00171 | Journal of the Endocrine Society | 1993–2011

the other components [2, 3], and its expression is markedly reduced in mice lacking the vitamin D receptor [4], suggesting that calcium entry across the brush border is the rate-limiting step in $1,25(OH)_2D$-regulated intestinal calcium transport. Thus, there is great interest in how this channel is regulated. Although induction of this protein by $1,25(OH)_2D$ is clearly one level of regulation, this mechanism would not suffice to adjust to rapid changes in the calcium content following meals. Patch clamp studies indicate that Trpv6 calcium channel activity is inhibited by high intracellular calcium levels [5, 6] mediated at least in part by calmodulin (CaM), which binds the channel in a calcium-dependent manner [7, 8]. In vitamin D–deficient animals, calcium accumulates just inside the brush border membrane [9, 10], and, therefore, would be expected to inhibit Trpv6 activity. Administration of $1,25(OH)_2D$ to vitamin D–deficient animals results in a flow of calcium out of the microvilli initially into vesicles and mitochondria in the terminal web [11, 12]. This initial flow of calcium following $1,25(OH)_2D$ administration occurs prior to and is independent of calbindin induction [13, 14], but coincides with increased CaM translocation into the brush border [15].

Most of the CaM in the brush border is bound to myosin 1A (Myo1a), a single-headed myosin previously thought to be expressed only in the intestinal epithelium that links the actin core of the microvillus to the plasma membrane [16]. In chicken intestine, $1,25(OH)_2D$ increases the amount of CaM binding to Myo1a without stimulating the production of either protein [17]. Myo1a is a mechanoenzyme with actin/Mg-activated ATPase activity that requires CaM and micromolar levels of calcium to function [18]. However, its role in the brush border remains poorly understood. We postulated that Myo1a plays a role in intestinal calcium transport by regulating the levels of CaM and calcium in the vicinity of Trpv6 and so controlling calcium flux through this channel. In this report, we show that overexpression of Myo1a in C2Bbe1 cells enhances while inhibition of Myo1a expression inhibits $1,25(OH)_2D$-stimulated intestinal calcium transport. Furthermore, Trpv6 forms a complex with Myo1a and CaM, suggesting a direct interaction among Myo1a, CaM, and Trpv6 to regulate calcium flux across the brush border. However, when we examined mice lacking Myo1a, we were unable to demonstrate a reduction in calcium transport, unlike what we observed in the *Trpv6*-null mouse, or to show that Myo1a deficiency further reduced calcium transport in *Trpv6*-null mice.

Decreased intestinal calcium transport is well known to result in osteopenia/osteoporosis (in calcium-deficient diets) or osteomalacia (in vitamin D–deficient diets). Thus, we examined the bones of the *Myo1a*- and *Trpv6*-null mice, anticipating that reductions in intestinal calcium transport would be reflected in changes in bone structure. Given the results of the intestinal transport studies, we expected the *Trpv6*-null mice to be osteopenia, but not the *Myo1a*-null mice. However, when we compared the bones of *Trpv6* and *Myo1a*-null mice, only the *Myo1a*-null mice showed an osteopenic phenotype. We then found that Myo1a was expressed in osteoblasts, unlike Trpv6, in which its lack led to decreased osteoblast differentiation. These surprising results suggest that at least in mice, Myo1a plays a greater role in regulating bone formation than it does in intestinal calcium transport, revealing a previously undiscovered role for Myo1a that had previously been thought to function only in the intestine.

1. Materials and Methods

A. Animals

Myo1a-null mice were a gift from Dr. Mark Mooseker. *Trpv6*-null mice were a gift from Dr. Matthias Hediger. These were back bred into a C57BL/6 background. The mice were then bred together to produce the double deletions. Control mice were C57BL/6 wild-type (WT) used for the back breeding. Both sexes were included in all studies. For calcium transport studies, the mice at weaning were placed on one of three diets differing only in calcium content (0.02%, 0.42%, and 2.0%; Teklad 248060, 248134, and 248161, respectively; Envigo, Somerset, NJ) for 2 weeks prior to study. For all other studies, the mice were raised on

standard mouse chow (Teklad 8656; Envigo) containing 1.2% calcium. The right tibias were obtained for micro-CT (μCT). The right distal femurs were obtained for trabecular bone histomorphometry and immunohistochemistry. Left tibias and femurs were obtained for mRNA determinations. Bone marrow stromal cells (BMSCs) from left tibias and femurs were collected from individual mice for cell culture. These studies were approved by the Animal Use Committee of the San Francisco VA Medical Center, where the animals were raised and studied.

B. μCT

The tibias were analyzed with a Scanco Medical AG μCT apparatus (Scanco Medical AG, Basserdorf, Switzerland) as previously described [19], following the guidelines developed by Bouxsein *et al.* [20]. Measurements were made in the proximal tibia for trabecular bone and just proximal to the tibiofibular junction for the cortical bone in 3-month-old mice.

C. Immunohistochemistry and Histomorphometry

To detect Myo1a expression by immunohistochemistry, the proximal tibia was fixed by 4% paraformaldehyde in PBS overnight at 4°C and decalcified by 10% EDTA. The decalcified tibias were then embedded in paraffin and cut into 5-μm sections. After deparaffinization and rehydration, the sections were quenched with 3% hydrogen peroxide in methanol for 15 minutes to block endogenous peroxidase activity. Nonspecific binding was blocked using 4% BSA in Tris-buffered saline for 30 minutes. Anti-Myo1a (Santa Cruz Biotechnology Inc., Santa Cruz, CA) [21] was applied to each section and incubated overnight at 4°C. The primary antibody was detected with the rabbit-specific HRP/DAB detection IHC kit (Santa Cruz Biotechnology, Inc., Santa Cruz, CA) [22] following the manufacturer's instructions. Negative controls were performed without the primary antibody. To assess trabecular bone volume (BV) and bone resorption, proximal tibial sections were stained by hematoxylin and eosin and by tartrate-resistant acid phosphatase (TRAP) staining for osteoclast detection. Trabecular BV/tissue volume (TV) and osteoclast number/bone surface (BS) were determined by BIOQUANT (BIOQUANT Image Analysis Corporation, Nashville, TN).

D. Western Blotting

C2Bbe1 cells were plated into six-well plates at 50,000 cells/cm^2 and allowed to grow to confluency. They were then infected with vector only or WT sense or antisense adenovirus constructs of the Myo1a–green fluorescent protein (GFP) clone at 1×10^7 plaque-forming units/cm^2. At 4, 7, 10, 13, 16, and 19 days postinfection, the cells were extracted in 200 μL RIPA extraction buffer (50 mM Tris-HCl, pH 7.4, 1% Triton X-100, 0.1% SDS, 150 mM NaCl, and 1 mM EDTA) containing Complete Protease Inhibitor Cocktail (Roche Applied Science, Indianapolis, IN) and 1 mM 4-(2-aminoethyl) benzenesulfonyl fluoride, HCl (Calbiochem, San Diego, CA). Samples were sonicated, centrifuged to spin out debris, and subjected to SDS-PAGE. Following electroblotting, the membranes were incubated in 1:5000 times chick gut Myo1a monoclonal antibody (MAB 1647; Chemicon International, Temecula, CA) [23], followed by 1:2000 times horseradish peroxidase–linked secondary antibody, incubation with SuperSignal West Dura Extended Duration Substrate (Pierce Protein Research Products, Rockford, IL), and autoradiography (BioMax MR; Kodak, Rochester, NY).

D-1. Cell culture

C2Bbe1. The C2Bbe1 clone of the cell line Caco2 (#CRL-2102; American Type Culture Collection, Manassas, VA) was used for studies of calcium transport *in vitro*. Depending on the experiment, these were plated on various support structures and grown in DMEM containing 4.5 g/L glucose, L-glutamine, and sodium pyruvate, penicillin/streptomycin

(Mediatech, Inc, Herndon, VA), 10% fetal calf serum (FCS; Atlanta Biologicals, Flowery Branch, GA), and 0.01 mg/mL transferrin (Gibco/Invitrogen, Carlsbad, CA). The cells were incubated at 37°C and 5% CO_2 until assayed. Specifics for each type of experiment are provided in the appropriate sections detailed later.

BMSCs. The left tibial and femoral BMSCs were harvested using techniques previously described [19]. Briefly, the tibias and femurs were collected, and the soft tissue and the epiphyses of each bone were removed. The bone marrow was flushed from the diaphysis with a syringe and a 26-gauge needle. The marrow from each individual mouse was collected in primary culture medium (α modification of Eagle medium containing L-glutamine and nucleosides; Mediatech) supplemented with 10% fetal bovine serum (Atlanta Biologicals), 100 U/mL penicillin/streptomycin (Mediatech), and 0.25 mg/mL Fungizone (Life Technologies, Rockville, MD). A single-cell suspension was obtained by repeated passage through an 18-gauge needle. A pool of BMSCs was made from the tibia and femur of each mouse. The cells were plated at 2×10^6 cells/well in six-well plates. Nonadherent cells were removed by aspiration, and then the primary medium was replenished on day 5. On day 7, the cells were provided with secondary medium [primary medium with 3 mM β-glycerophosphate (Sigma-Aldrich, St. Louis, MO) and 50 mg/mL ascorbic acid (Sigma-Aldrich)]. Subsequent medium changes were performed every 2 days for up to 21 days.

E. Adenoviral Constructs of Myo1a

The coding region sequence of Myo1a, previously cloned into the pEGFP-N1 vector (Clontech, Palo Alto, CA), was released from the vector, along with the coding region for GFP, using *Sac*I and *Dra*I restriction digestion (New England Biolabs, Beverly, MA) and then subcloned into pAxCAwt using the manufacturer's protocols (Takara Bio, Madison, WI). A 1-μL aliquot of the ligated sample was packaged using a Gigapack III XL kit (Stratagene, La Jolla, CA) and transfected into nonchemically competent DH5α cells (Clontech). PCR was used to confirm the orientation of insert in either the sense or antisense direction. A forward primer for the pAxCAwt vector (P1: 5′-ACGTGCTGGTTGTTGTGCT-3′) was combined with a reverse primer for the 5′ end of the Myo1a-GFP insert (S5: 5′-AATTGTTGTTGCGAATGGT-3′) or a reverse primer for the 3′ end of the Myo1a-GFP insert (AS5: 5′-AGCTGAAGGGCATCGACTT-3′). If the insert is in the sense direction, the P1/S5 primer set will yield a 522-base pair product. If in the antisense orientation, the P1/AS5 primer set will yield a 460-base pair product. Similarly, a reverse primer on the pAxCAwt vector (P2: 5′-TCCTTCCGAGTGAGAGAC-3′) was combined with a forward primer from the 3′ end of the Myo1a-GFP (S3: 5′-GAGGACGGCAACTACAAG-3′) or a forward primer from the 5′ end of Myo1a-GFP (AS3: 5′-ATTTGCCAATGCGTAGAT-3′). If the insert is in the sense direction, the P2/S3 primer set yields a 725-base pair product. If inserted in the antisense direction, the P2/AS3 primer set yields a 500-base pair product. A midscale cosmid prep was prepared from selected positive clones using the QIAfilter Midi Kit (Qiagen, Valencia, CA) and transfected into HEK293 cells using the manufacturer's protocols (Takara Bio). Those wells showing lysis between days 10 and 13 were collected as clones. Each clone was tested for replication deficiency by infecting both HEK293 cells and HeLa cells. Those clones that lysed the HEK293 cells but did not lyse the HeLa cells were considered replication deficient. These clones were multiplied through four seedings according to the manufacturer's protocol and the virus collected and stored at −80°C ready for use.

F. Colocalization

C2Bbe1 cells were seeded into 12-mm diameter Transwell Clear Permeable Supports, 0.4-μm pore size (Costar; Corning, Corning, NY) at a density of 50,000 cells/well in growth media [DMEM plus 4.5 g/L glucose, L-glutamine, and sodium pyruvate plus penicillin/streptomycin (Mediatech, Carlsbad, CA) with 10% FCS (Atlanta Biologicals, Flowerly Branch, GA) and 0.01 mg/mL transferrin (Gibco/Invitrogen)]. The cells were incubated at 37°C and 5% CO_2 until confluency. The cells were then infected with adenovirus constructs for Myo1a-GFP at

1×10^7 plaque-forming units/cm^2. After 7 days of incubation, the cells were rinsed in calcium/magnesium-free PBS and fixed in 3.7% formaldehyde in PBS. Cells were then permeabilized with 0.1% Triton X-100 followed by counterstaining for actin with Texas Red–phalloidin (Molecular Probes, Eugene, OR). The Transwell membrane was then cut away from the insert and mounted on a microscope slide. Samples were examined by confocal microscopy for the presence of GFP-labeled Myo1a and Texas Red–labeled actin. Computer-generated x-z sections were generated and overlay images produced in Photoshop (Adobe Systems, San Jose, CA).

G. TRPV6 Antibody Production

In preparation for the coimmunoprecipitation and western blotting experiments, we generated an antibody to human TRPV6. The antibody was raised in rabbits against the TRPV6 peptide sequence NH3-SEDLDKDSVEKLELGC-COOH (ImmunoVision Technologies, Brisbane, CA) [24]. This epitope corresponds to amino acids 656 to 671 of the human TRPV6 sequence (GeneBank accession number AAG41951.1). The second production bleed was affinity purified against the peptide prior to use in western blots and immunoprecipitation.

H. CoImmunoprecipitation

C2Bbe1 cells were seeded and allowed to grow for 10 days postconfluence. The standard growth media with 10% FCS was replaced with the same media containing 5% FCS. Cells were treated with 1×10^{-8} M 1,25 $(OH)_2D_3$ in 0.1% ethanol or vehicle for 72 hours, replacing media and retreating every 24 hours. At harvest, cells were rinsed two times with calcium/magnesium-free PBS, scraped into PBS containing protease inhibitors, transferred to a dounce homogenizer on ice, and homogenized with 15 strokes. Each sample was centrifuged at 100,000*g* for 30 minutes at 4°C. The pellet was extracted in 1% Nonidet P-40, 2 mM EDTA, 150 mM NaCl, and 50 mM Tris, pH 8.0 (Sigma-Aldrich), containing Complete Protease Inhibitors (Roche) and 1 mM 4-(2-aminoethyl) benzenesulfonyl fluoride, HCl (Calbiochem) using dounce homogenization. The sample was spun at 16,000*g* to remove insoluble material, precleared with A/G PLUS Agarose beads (Santa Cruz Biotechnology, Inc.), and then incubated overnight with either 1:500 times anti-chick gut Myo1a monoclonal antibody as noted previously or 1:500 times anti-TRPV6 rabbit polyclonal antibody. A/G PLUS Agarose beads (Santa Cruz Biotechnology, Inc.) were added to the samples and tumbled 1 hour at 4°C. The beads were washed and then extracted in 15 μL two times sample loading buffer (625 mM Tris, pH 6.8, 20% glycerol, 20% SDS, and 0.1% bromophenol blue) prior to SDS-PAGE. The blots were then probed for Myo1a, TRPV6, or CaM (1:800 CaM-FL rabbit polyclonal Ab; Santa Cruz Biotechnology, Inc.) [25] and the signal detected as described previously.

I. Calcium Transport

In vitro, C2Bbe1 cells were seeded onto 24-mm, 0.4-μm pore Transwell Clear tissue culture inserts (Costar; Corning) at 250,000 cells/well in 1.5 mL growth media per inner well and 2.0 mL growth media per outer well. At confluence, the cells were infected with adenovirus constructs for Myo1a-GFP sense or antisense or vector only at 1×10^7 infectious particles/cm^2. Cells were incubated at 37°C and 5% CO_2. On day 11 postinfection, the medium was removed and replaced with 5% FCS containing media in both the inner and outer well. Cells were treated with 1×10^{-8} M 1,25$(OH)_2D_3$ in 0.1% ethanol or vehicle for 72 hours, replacing media and treatments in both inner and outer wells every 24 hours. Calcium transport was measured using the method of Fleet and Wood [26].

I-1. In vivo

The ligated *in situ* duodenal loop technique was used as we previously described [15]. Three centimeters of the proximal portion of the duodenum is exposed, flushed with saline, ligated

to form a loop with blood supply intact, and then injected with 100 μL PBS containing 1 μCi ^{45}Ca in 1 mM calcium. Fifteen minutes later, at the time of euthanasia, the blood was obtained by cardiac puncture and assessed for ^{45}Ca. The data are expressed as: (counts per minute)/20 μL serum/(counts per minute/20 μL loop media) × 10,000.

J. Quantitative PCR

Total RNA was extracted from the BMSCs, intestinal mucosa, and tibial shaft (marrow flushed out). The RNA was reversed transcribed into cDNA as previously described and quantitated using the SYBR reagent or commercially obtained or custom-designed primers and probes from Applied Biosystems using the Applied Biosystems 7900 HT (Foster City, CA) as previously described [19, 27].

Quantitative polymerase chain reaction (QPCR) primer sets were: 1) Myo1a: forward primer, 5′-ACCAGAGTTCATTGCCAAATACCGGGACTA-3′ and reverse primer, 5′-ACGTAGGACATCACTAGCTTACTCGCCTCA-3′; 2) Trpv6: primers and probe ordered from Applied Biosystems (MM00499078-M1); 3) GAPDH: forward primer, 5′-TGCACCACCAACTGCTTAG-3′ and reverse primer, 5′-GGATGCAGGGATGATGTTC-3′; 4) L19: forward primer, 5′-CCAAGAAGATTGACCGCCATA-3′, reverse primer: 5′-GTCAGCCAGGAGCTTCTTGC-3′, and probe, Fam-CATCCTCATGGAGCACATCCACAA-BHQ; 5) alkaline phosphatase (AP): forward, 5′-TCCTGACCAAAAACCTCAAAGG-3′, reverse, 5′-TGCTTCATGCAGAGCCTGC-3′, and probe, 5′-CTGGTGGAAGGAGGCAGGATTGACC-3′; 6) osteocalcin (OCN): forward, 5′-CTCACAGATGCCAAGCCCA-3′, reverse, 5′-CCAAGGTAGCGCCGGAGTCT-3′, and probe, 5′-CCCTGAGTCTCTGACAAAGCCTTCATGTCCA-3′; and 7) CaM: forward, 5′-GTGGATGCTGATGGTAATGGC-3′ and reverse, 5′-TTCTCTGATCATTTCATCTACTTCTTCAT-3′.

K. Determination of AP-Positive Colony Number and Calcium Nodule Formation

BMSCs were grown in six-well plates for up to 21 days. At day 7 of culture, the number of colony-forming units (CFUs) per plate was determined. At day 14 of culture, cells were fixed by 10% neutral buffered formalin and assessed using Sigma 104 Phosphate Substrate (Sigma-Aldrich) to determine alkaline phosphatase (AP)-positive CFUs following the manufacturers' instructions. At day 21 of culture, calcium nodules were fixed by 10% neutral buffered formalin and stained with 2% Alizarin Red (Sigma-Aldrich) for 10 minutes. The stain was aspirated and the dishes rinsed five times with distilled water to remove loosely bound stain. The number of mineralized nodules was determined, and the specifically bound stain was eluted with a solution of 10% cetylpyridinium chloride (CPC) and quantitated in a spectrophotometer at 540 nm.

L. Statistical Analysis

Data are presented as mean ± SD. For the calcium transport studies, two-way ANOVA was used. For the μCT studies, one-way ANOVA was used. Comparisons between genotypes for mRNA and cell culture results were analyzed by Student *t* test. Statistical significance was stated for P values <0.05.

2. Results

A. Effect of Myo1a on Calcium Transport in vitro

To determine whether alterations in Myo1a levels would impact 1,25(OH)$_2$D-regulated intestinal calcium transport, we prepared an expression vector for Myo1a in the sense and antisense direction. We plated C2Bbe1 cells on transwells and infected them with these constructs when confluent. Control cells were infected with the empty adenovirus vector. Figure 1 demonstrates that the sense construct localized appropriately to the brush border membrane and that the sense construct increased and antisense construct decreased

Myo1a expression in these cells. The endogenous Myo1a is seen as a 110-kD band, and the GFP-Myo1a construct runs at 145 kD. The faint 125-kD band is not specific. The endogenous Myo1a increased with time after confluence in the control (WT) cells, but this was blocked by both the antisense construct and sense construct. Although the inhibition of endogenous Myo1a by the antisense construct is the expected result, its inhibition by the sense construct even after it no longer expressed Myo1a is unclear. This could represent prolonged inhibition of endogenous Myo1a expression by the initially elevated Myo1a levels or a nonspecific action of the viral construct itself. Overexpression of the sense construct was maximal by 4 to 7 days after infection and decreased with time. Calcium transport across these cells was measured on day 14 postinfection, following a 3-day period during which 10^{-8} M $1,25(OH)_2D$ or its vehicle (ethanol) was administered daily. The time following infection to measure calcium transport was chosen to ensure both adequate endogenous Myo1a expression in the vector only cells and only a modest overexpression of Myo1a in the overexpressing cells. The experiments shown in Fig. 2 are representative of three separate experiments for each condition, each performed with different preparations of C2Bbe1 cells. $1,25(OH)_2D$ stimulated calcium transport in the vector-infected cells by fourfold to eightfold. Overexpression of Myo1a increased basal and $1,25(OH)_2D$-stimulated calcium transport by ~50%. These increases were significant ($P < 0.01$). The antisense construct had no effect on basal calcium transport, but inhibited $1,25(OH)_2D$-stimulated calcium transport by ~80% ($P < 0.02$). In the vector only–treated cells, $1,25(OH)_2D$

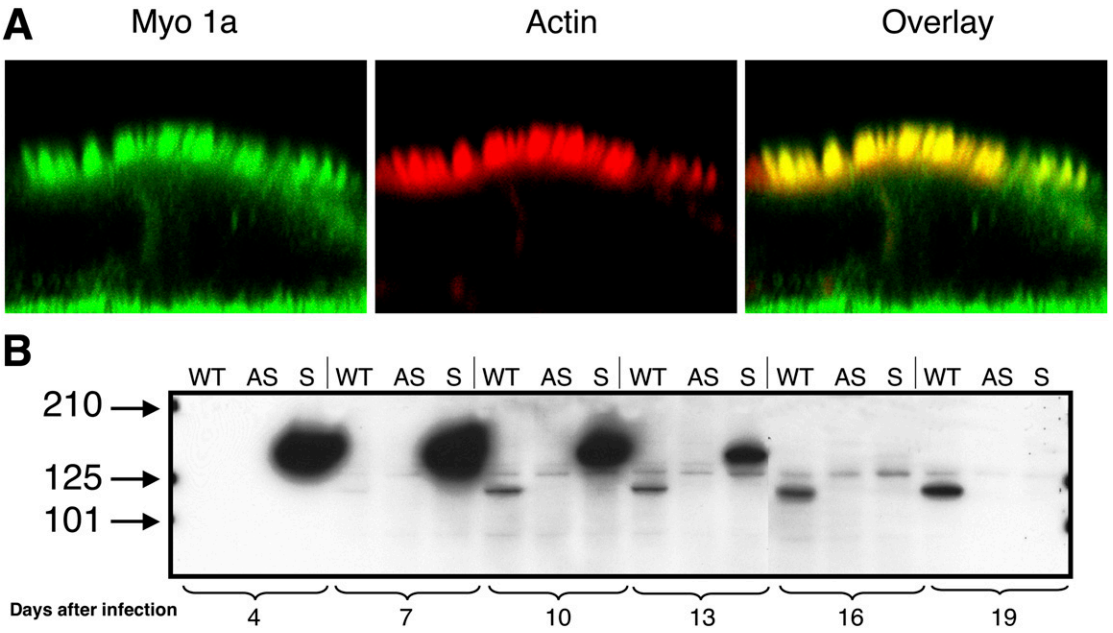

Figure 1. (A) Myo1a colocalizes with actin in the brush border of intestinal epithelial cells. C2Bbe1 cells were grown on Transwell inserts. At confluency, they were infected with adenoviral constructs expressing full-length Myo1a fused with GFP. After 7 d, the cells were stained with Texas Red–phalloidin to label actin and examined by confocal microscopy. Myo1 colocalized with actin in the brush border. (B) Myo1a sense constructs increase while antisense constructs of Myo1a decrease Myo1a expression in a time-dependent fashion. C2Bbe1 cells were grown to confluency and then infected with vector only (WT), a full-length antisense construct (AS), or the full-length Myo1a-GFP fusion construct (S). At the indicated times, the levels of Myo1a were determined by western analysis. The Myo1a-GFP fusion protein is expressed as a 145-kD protein, whereas the endogenous Myo1a is expressed as a 110-kD protein. The antisense Myo1a construct blocks endogenous Myo1a production, whereas the sense Myo1a-GFP construct overexpresses the full-length Myo1a-GFP fusion protein. This experiment was repeated twice with consistent results.

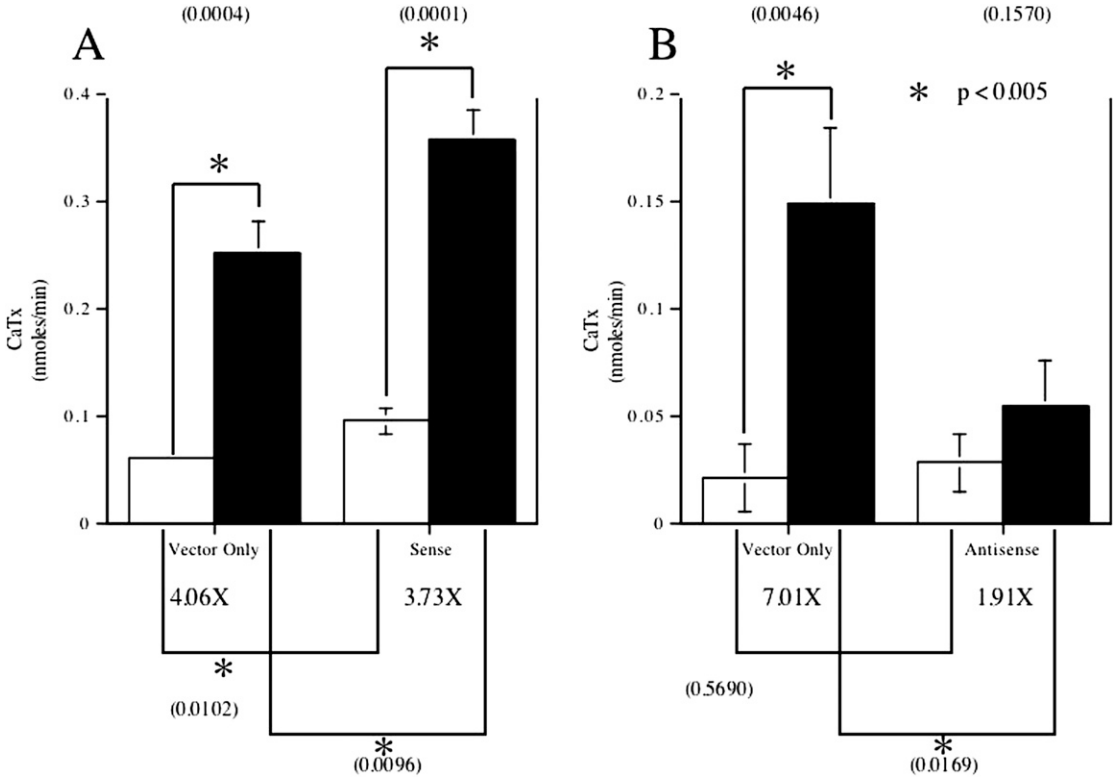

Figure 2. Overexpression of Myo1a enhances while inhibition of Myo1a expression blocks $1,25(OH)_2D_3$-stimulated calcium transport. C2Bbe1 cells were grown to confluency on Transwell inserts and then infected with vector only or the sense and antisense constructs of Myo1a. After 11 d, the media was replaced and the cells treated with 10 nM $1,25(OH)_2D_3$ daily for 3 d, at which point calcium transport (CaTx) was measured as described in experimental procedures. $1,25(OH)_2D_3$-stimulated calcium transport was increased by overexpression of Myo1a (which also increased basal calcium transport) but was blocked by inhibition of Myo1a expression using the antisense construct. The error bars enclose mean ± SD of triplicate determinations. The white bars represent the vehicle-treated cells, and the black bars are the cells receiving $1,25(OH)_2D_3$. The experiment was repeated twice with consistent results. $^*P < 0.01$ compared vehicle-treated cells.

stimulated Trpv6 expression sevenfold, but did not increase the expression of either Myo1a or CaM (Fig. 3).

B. Myo1a Forms a Complex With CaM and TRPV6

To determine whether Myo1a formed a complex with TRPV6 to enhance its ability to transport calcium, C2Bbe1 cells were treated for 72 hours with 10^{-8} M $1,25(OH)_2D$ or vehicle (ethanol) beginning on day 10 postconfluence. The cells were then lysed, the membrane extract immunoprecipitated with an antibody to Myo1a or TRPV6, and the immunoprecipitates evaluated by western analysis for TRPV6, CaM, and Myo1a (Fig. 4). The TRPV6 antibody recognizes a protein of ~85 kDa, although higher molecular weight forms are sometimes seen, which are thought to represent different glycosylated forms of TRPV6 [6, 8]. The CaM antibody recognizes a 22-kDa band, indicating a low content of calcium in the CaM preparation, although the breadth of the band indicates some residual calcium that affects it migration in the gel [18]. The Myo1a antibody recognizes predominantly the 110-kDa band described previously. Nonspecific IgG brought down none of these proteins (data not shown). $1,25(OH)_2D$ increased the total amount of TRPV6 and CaM in the lysate, but not that of Myo1a. The major point, however, is that immunoprecipitation with an antibody to Myo1a coimmunoprecipitated CaM and TRPV6, as did the antibody to TRPV6 coimmunoprecipitate Myo1a and CaM.

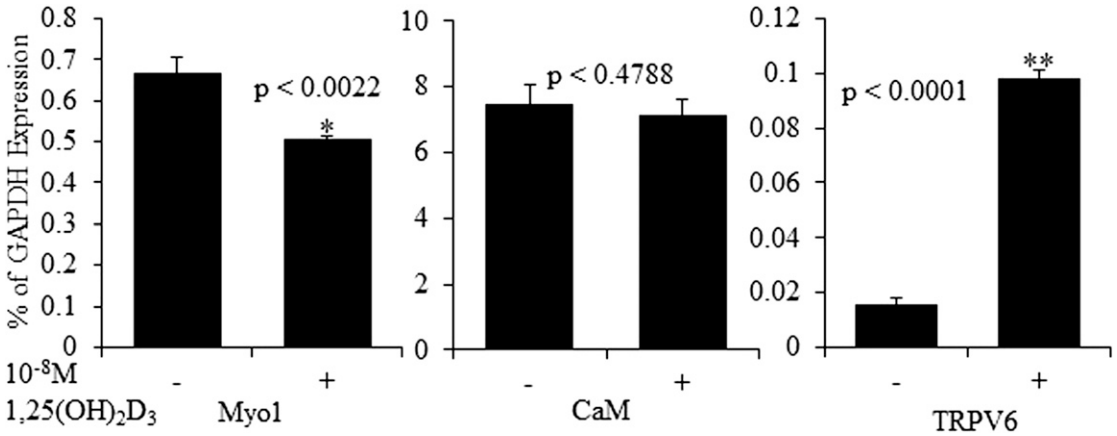

Figure 3. $1,25(OH)_2D_3$ stimulates TRPV6 expression but not Myo1a or CaM expression. C2Bbe1 cells were grown to 12 d postconfluency and then treated with 10 nM $1,25(OH)_2D_3$ for 24 h. The RNA was extracted and analyzed for mRNA levels of Myo1a (BBM1), CaM, Trpv6, and GAPDH using real-time QPCR. $1,25(OH)_2D_3$ increased Trpv6 mRNA levels nearly sevenfold, with no effect on CaM mRNA levels and a 25% reduction in Myo1a (BBM1) mRNA levels. The error bars enclose mean ± SD of triplicate determinations. Lack of an error bar indicates an SD too small to be charted. The experiment was repeated twice with consistent results. *$P < 0.01$ compared with vehicle treatment; **$P < 0.001$ compared with vehicle treatment.

B-1. Myo1a deletion unlike Trpv6 deletion failed to impact intestinal calcium transport in vivo

To determine whether Myo1a was required for intestinal calcium transport *in vivo*, perhaps in synergism with Trpv6, we examined intestinal calcium transport in single *Myo1a*- and *Trpv6*-null mice and double-null mice at three different calcium concentrations (0.02%, 0.42%, and 2.0%). The mRNA levels in the intestine of the Myo1a-null and Trpv6-null mice are shown in Fig. 5, demonstrating that the respective deletion of these genes is essentially complete (undetectable). The mice were put on one of three calcium diets at weaning for 2 weeks prior to study. The results are shown in Fig. 6. The control mice did not show a considerable decrease in calcium transport with the increase in dietary calcium, likely reflecting the limited period (2 weeks) in which they were on the different calcium diets. There was no notable reduction of calcium transport at the 0.02% and 0.42% calcium diet level in the *Myo1a*-null mice compared with controls, although calcium transport was slightly but significantly reduced on the 2% calcium diet. These results are in contrast to the marked reduction in calcium transport in the *Trpv6*-null mice when fed the 0.42% and especially the 2% calcium diet. Furthermore, lack of Myo1a did not alter the results in the *Trpv6*-null mice. These results stand in contrast to the human intestinal cell line C2Bbe1, in which overexpression and underexpression of Myo1a increased and decreased $1,25(OH)_2D$-stimulated calcium transport, respectively, and an interaction between Myo1a and Trpv6 could be demonstrated.

C. Myo1a Deletion But Not Trpv6 Deletion Leads to Osteopenia

To determine whether these differences in intestinal calcium transport in the *Myo1a*- and *Trpv6*-null mice had implications for the skeleton, we examined the tibiae and femora of these mice at 3 months of age. At this time point, the *Trpv6*-null mice were comparable to controls in terms of body weight, but the *Myo1a*-null and double-null mice were 15% and 22% smaller, respectively, than the controls. The μCT results are shown in Fig. 7. The bones of the *Myo1a*-null mice were smaller than their WT controls, as assessed by a 20% to 24% reduction in both trabecular and cortical total volume, consistent with their reduced body weights. The bones

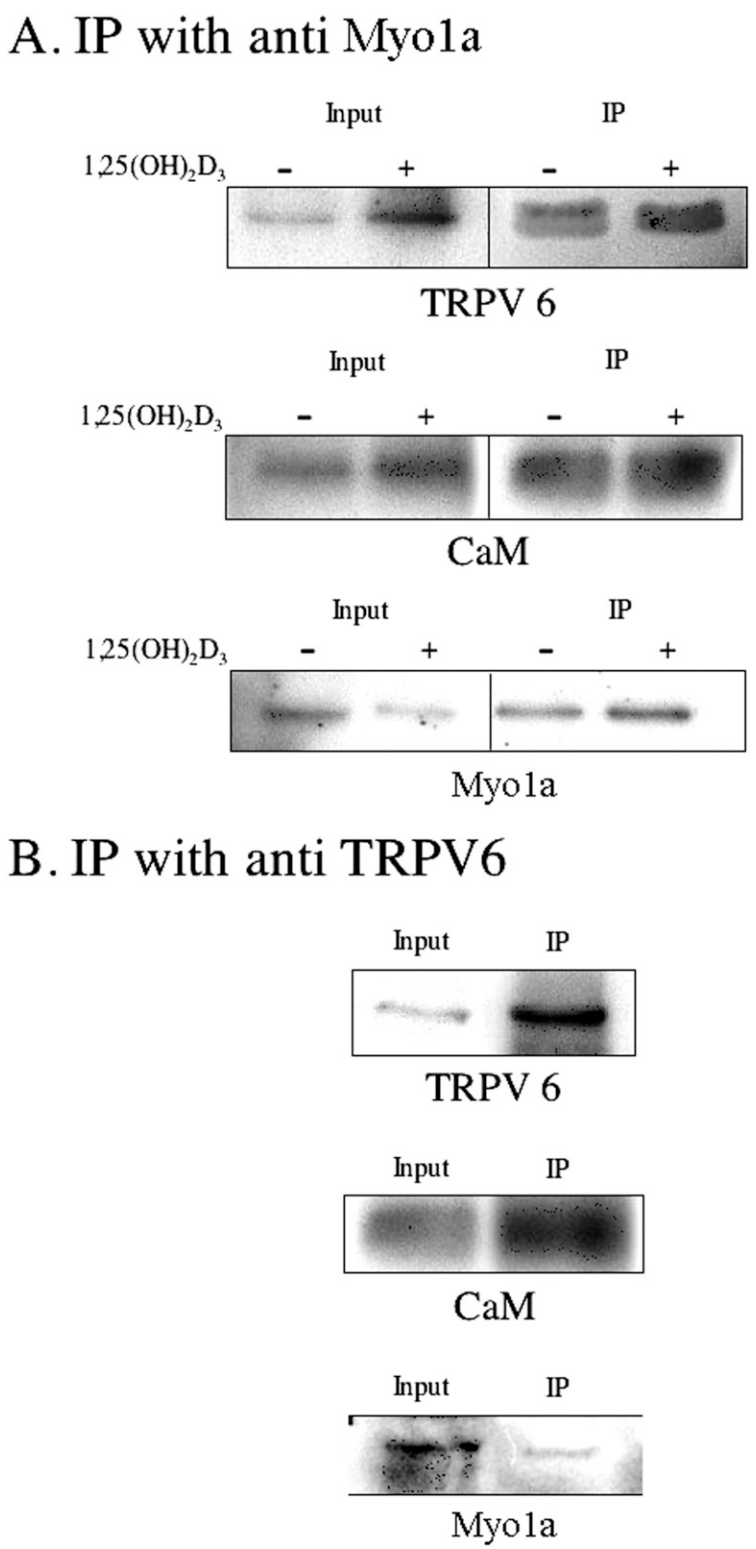

Figure 4. Myo1a forms a complex with TRPV6 and CaM. C2Bbe1 cells were grown to 10 d postconfluence then treated daily for 3 d with 10 nM $1,25(OH)_2D_3$. At this point the cells were lysed, centrifuged, and the 100,000*g* pellet extracted with 1% Nonidet P-40–containing buffers as described in Materials and Methods. This extract was immunoprecipitated (IP) with an antibody to (A) Myo1a or (B) TRPV6 and the IP analyzed for TRPV6, CaM, and Myo1a. Both TRPV6 and CaM were coimmunoprecipitated with Myo1a in either case. $1,25(OH)_2D_3$ increased the levels of TRPV6 and CaM and decreased the levels of Myo1a in the membrane lysate but did not have a major impact on the ratio of these proteins in the IP. This experiment was repeated three times with comparable results.

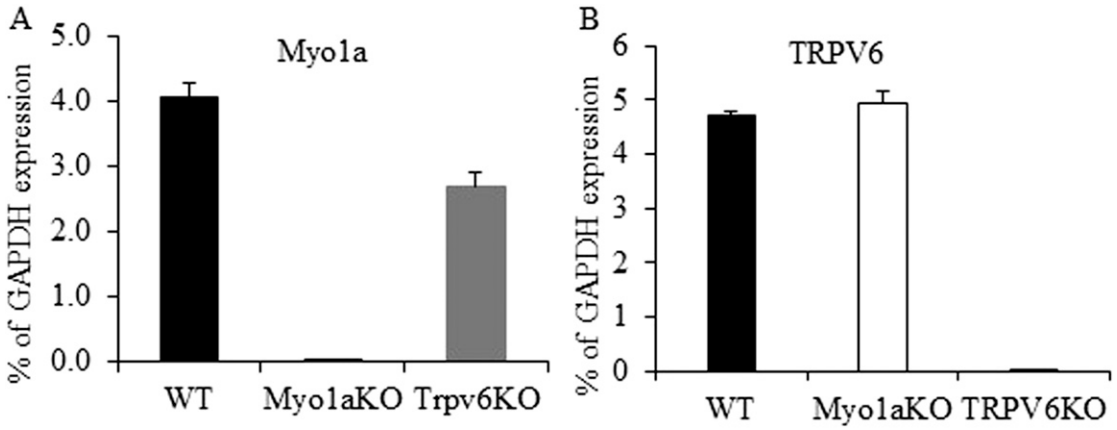

Figure 5. mRNA levels of Trpv6 and Myo1 are undetectable in the intestine of the respective KO mice but robust in WT controls. The mRNA levels of Trpv6 and Myo1a from the duodenal mucosa of 6 wk control (WT) and KO mice were measured by real-time QPCR. In the respective KO mice, the mRNA levels of Trpv6 or Myo1a were undetectable with robust expression in the controls. Results are expressed as mean ± SD of triplicate determinations from two different mice of each genotype. WT, black bars; Myo1a KO, white bars; and Trpv6 KO, gray bars.

from the *Trpv6*-null mice were not reduced in size relative to the WT controls and were even slightly but significantly larger in the cortical bone. In the *Myo1a*-null mice trabecular BV/TV was reduced 53%. Trabecular number was reduced by 16%, trabecular thickness by 23%, and connectivity density by 64%. Cortical TV and BV were each reduced by equivalent amounts (24% and 22%, respectively) such that BV/TV was not significantly altered. Cortical thickness, likewise, was not significantly reduced [mean ± SD, WT: 0.26 ± 0.02 mm; Myo1aKO:

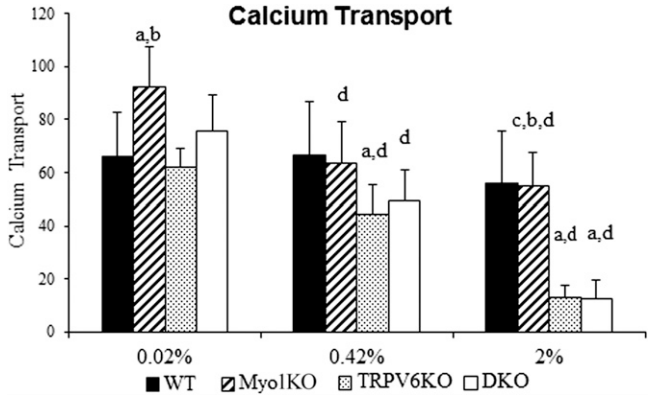

Figure 6. Intestinal calcium transport was reduced in Trpv6 KO and DKO mice but not Myo1a KO mice. At weaning, the mice were placed on one of three diets (0.02%, 0.42%, and 2.0%) for 2 wk prior to evaluating calcium transport across the duodenum using the ligated loop method. N = 3 for each group on each diet. Only the Trpv6 KO and DKO mice showed a reduction in calcium transport relative to controls, best seen at the higher dietary calcium. Error bars enclose mean ± SD. Data are expressed as a ratio of the counts in serum to the counts in the ligated loop × 10,000. The data were analyzed by two-way ANOVA. [a]In the same diet, significant difference from WT; [b]in the same diet, significant from TRPV6KO; [c]in the same diet, significant when compared with DKO; [d]in the same genotype, significant when compared with 0.02% diet.

0.24 ± 0.02 mm; TRPV6 knockout (KO): 0.25 ± 0.02 mm; and double KO (DKO): 0.24 ± 0.02 mm], but the medullary volume of the Myo1a KO was reduced 31%. These data suggest that the Myo1a KO favors endosteal to periosteal bone growth in comparison with controls and the Trpv6 KO. The tibiae of the *Trpv6* null mice, in contrast, did not show these reductions, but rather were found to have higher BVs than controls with trabecular BV/TV increased 80%, trabecular thickness increased 26%, and connectivity density by 112%. Cortical BV and TV were increased 8% and 19%, such that the BV/TV was actually less than control. Cortical thickness was not significantly altered but medullary volume was increased 42%, indicating that unlike the Myo1a KO, periosteal expansion was favored. The skeletal measurements in the DKO mice were not significantly different from those in the *Myo1a*-null mice, indicating that the lack of Myo1a eliminated any impact on the skeleton induced by lack of Trpv6. These results were very surprising, as up to now, Myo1a was thought to be restricted to the intestinal epithelium, and our results with intestinal calcium transport led us to anticipate that the *Trpv6*-null, not the *Myo1a*-null, mice would have the reduction in bone. Thus, we further examined bone to determine whether Myo1a was expressed there and, if so, what role it played.

D. Localization and Function of Myo1a in Osteoblasts

To determine whether Myo1a is expressed in bone, immunohistochemistry using an antibody against Myo1a was performed in the tibial sections of WT and Myo1a-null mice. As shown in Fig. 8A, Myo1a is expressed in the osteoblasts on the BS and osteocytes embedded in bone matrix in the tibias of the WT mice (Fig. 8A, WT), but the expression was abolished in the Myo1a-null mice (Fig. 8A, KO). Consistent with the μCT measurements, histomorphometry showed that the trabecular BV in the *Myo1a*-null mice (Fig. 8B, KO) was remarkably reduced when compared with the WT mice (Fig. 8B, WT). In contrast, by TRAP staining, osteoclast morphology was not altered in the *Myo1a*-null mice (Fig. 8C, KO) when compared with the WT mice (Fig. 8C, WT). Quantitation of these data are shown in Fig. 8D. As shown in Fig. 8D, TV (−29%), BV (−73%), and BV/TV (−63%) were significantly decreased in the *Myo1a*-null mice when compared with the WTs, confirming the bone loss in these mice. Compared with the WTs, BS (−65%) and total osteoblast number (−65%) were remarkably decreased in the *Myo1a*-null mice, although the osteoblast number/BS was comparable. Osteoclast number/BS was likewise comparable in the WTs and KOs when normalized to BS, although overall number was reduced given the reduced BS.

To further confirm the expression of Myo1a in bone, we isolated RNA from the tibia and femur (marrow flushed out) and determined the mRNA levels of Myo1a by QPCR. As shown in Fig. 9A, mRNA of Myo1a was expressed in the bones of WT mice (Fig. 9A, solid bars), but essentially none in the bones of the *Myo1a*-null mice. In addition, no Trpv6 mRNA was found by QPCR in the bones from either WT mice or *Myo1a*-null mice (Fig. 9A, open bars). To investigate the role of Myo1a in osteoblast differentiation, bone mRNA levels of AP and OCN were determined by QPCR. Compared with the WT mice, a trend (not significant) toward a reduction in mRNA levels of AP (Fig. 9B) and a marked reduction (50%) of mRNA levels of OCN (Fig. 9C) were observed in the Myo1a-null mice. Runx2, RANK ligand, and RANK mRNA levels were not significantly different (data not shown). These results suggest that Myo1a stimulates the latter stages of osteoblast differentiation. To examine directly the effects of Myo1a on osteoblast differentiation, BMSCs (osteoblast progenitors) were cultured *in vitro* up to 21 days (Fig. 10). At day 7, there were no differences in CFUs (CFUs in WT, 15 ± 2; KO, 19 ± 5). At day 14 of BMSC culture, 40% fewer AP-positive colonies were formed in the cultures from *Myo1a*-null mice than in the cultures from the WT mice (Fig. 10A). In addition, at day 21 of BMSC culture, mineralization was also impaired in the cultures of the *Myo1a*-null mice (Fig. 10B). The number of mineralized nodules and mineral content (eluted by 10% CPC) was reduced by 76% and 88%, respectively, in the null mice cultures compared with the WT cultures, confirming the QPCR results that Myo1a in osteoblasts is required for their differentiation.

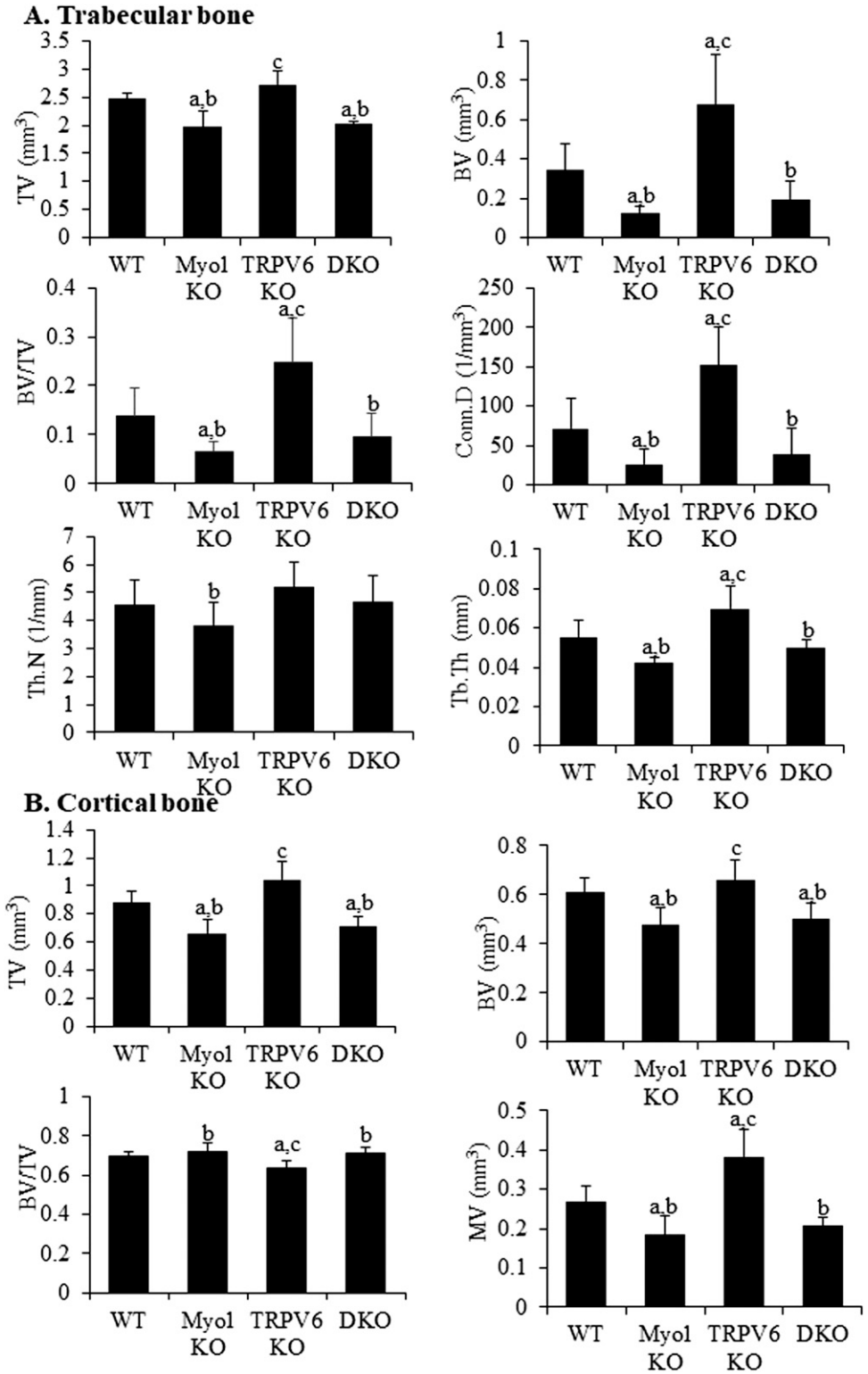

Figure 7. Myo1a KO and DKO mice showed a reduction in (A) trabecular and (B) cortical bone, but Trpv6 mice did not. The tibiae were obtained at 3 mo of age and their structures assessed by μCT. The *Myo1a*-null but not the *Trpv6*-null showed a reduction in bone compared with controls. N = 6–12 for each genotype. One-way ANOVA was used to analyze the results. The data are expressed as mean ± SD. [a]Significantly different from WT; [b]significantly different from TRPV6 KO; [c]significantly different from DKO. Conn.D, connectivity density; MV,marrow volume; Tb.Th, trabecular thickness; Th.N, trabecular number.

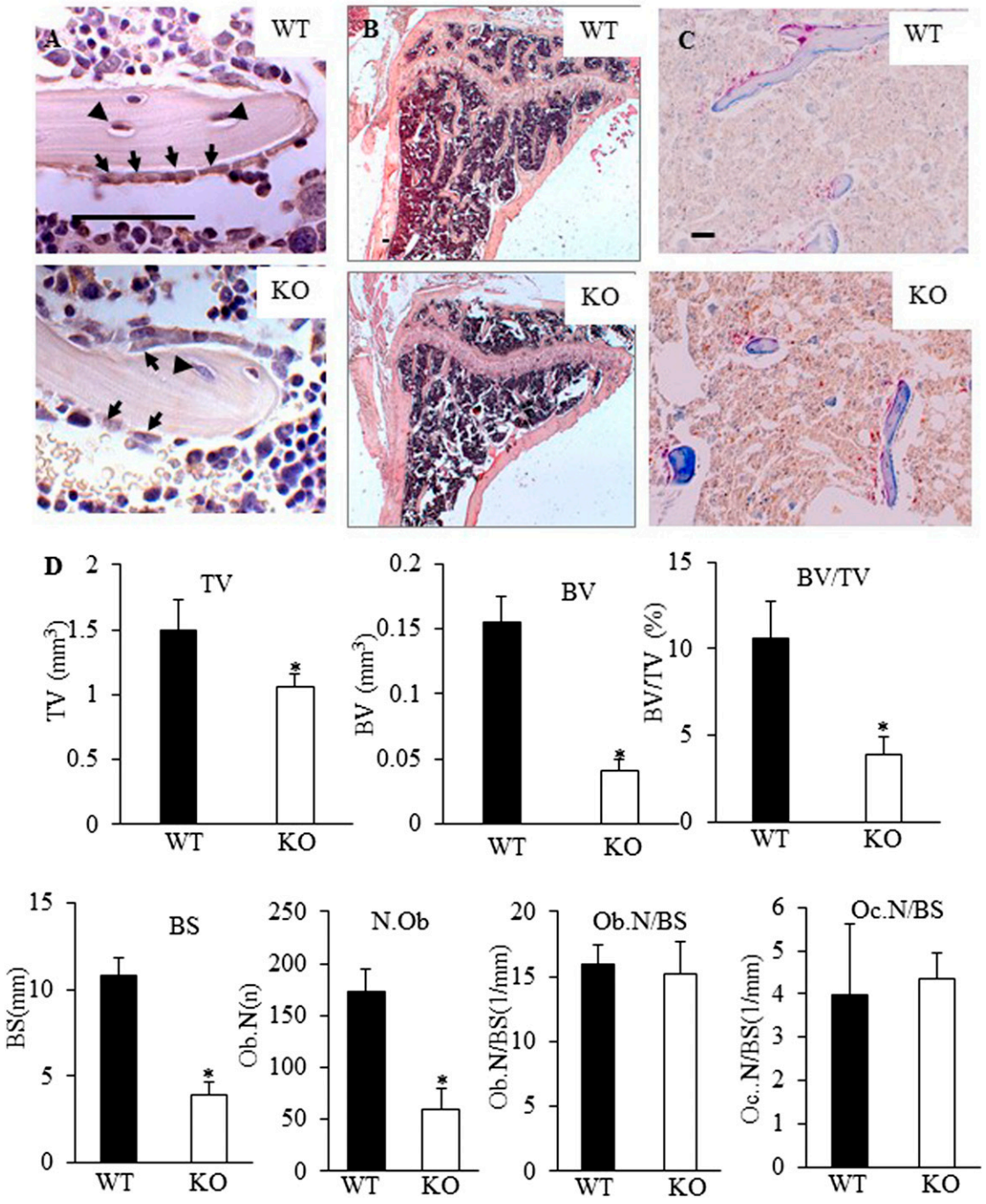

Figure 8. Expression of Myo1 in osteoblasts and the impact of its deletion on bone histomorphometry. (A–C) Representative figures of WT (top) and KO (bottom) mice. (A) Immunohistochemistry using an antibody against Myo1a identified Myo1a (brown) in the osteoblasts (arrows) along the BS and osteocytes (arrowheads) within cortical bone in the WT (top) mice, but the expression was abolished in the Myo1aKO (KO) mice. (B) Histomorphometry confirmed that the trabecular BV was decreased in the KOs (bottom) when compared with the WTs (top). (C) TRAP staining showed that the number of osteoclasts (pink) in the BS was comparable in the WTs (top) and KOs (bottom). (A) Magnification ×40 and (C) ×10 (scale bars, 50 μm); (B) ×5 (scale bar, 100 μm). (D) Trabecular bone histomorphometry measurements of WT (black bars) and KO (white bars). *$P < 0.05$ WT vs KO. Ob.N, osteoblast number; Oc.N, osteoclast number.

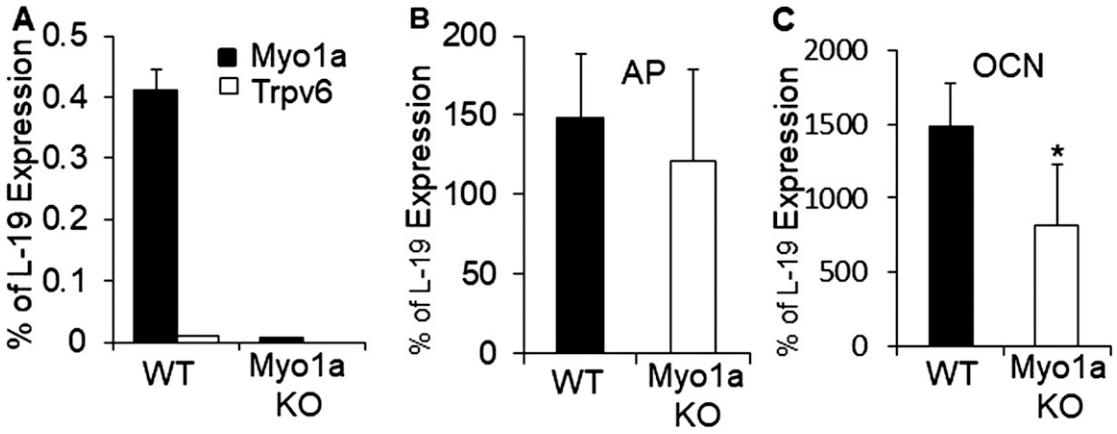

Figure 9. Bone expresses Myo1a but not Trpv6. Deletion of Myo1a reduces the expression of OCN. mRNA levels from the tibial shaft of control and Myo1a 3-mo-old mice were measured by real-time QPCR. (A) mRNA levels of Myo1a (black bars) and Trpv6 (white bars) in the WT and Myo1aKO mice. Myo1a was expressed in the WT mice, but was completely eliminated in the Myo1aKO mice. No Trpv6 expression was found by QPCR in either WTs or Myo1aKOs, indicating Trpv6 is not expressed in bone. mRNA levels of (C) OCN were significantly decreased in the Myo1aKOs (white bars) when compared with the WTs (black bars), while no changes were observed in the mRNA levels of (B) AP between WTs and KOs. Results are expressed as percentage of L-19 (housekeeper gene) (mean ± SD). n = 5 for WT; n = 3 to 4 for KO. *$P < 0.05$ vs WT.

3. Discussion

This study began as an evaluation of the role of Myo1a in regulating intestinal calcium transport, a role we hypothesized would involve regulation of the intestinal calcium channel Trpv6. Trpv6 is well established as a $1,25(OH)_2D$-regulated calcium channel in the intestinal brush border [1–3, 28], although its deletion does not prevent all of the $1,25(OH)_2D$-stimulated active transport [29]. Studies with HEK293 cells or frog oocytes overexpressing Trpv6 demonstrate its regulation by calcium, and this regulation appears to be mediated, at least in part, by CaM, which binds to Trpv6 in a calcium-dependent fashion and inhibits its activity. Trpv6 is expressed at highest levels in the apical regions of the intestinal villus [30, 31]. This is the same region where we [32] showed the greatest level of calcium-accumulating ability by brush border membrane vesicles and highest levels of CaM and Myo1a in the brush border. Therefore, we wanted to determine whether there was a link between the increased binding of CaM to Myo1a in the brush border following $1,25(OH)_2D$ administration and Trpv6 regulation. Important for this concept is that earlier studies of vitamin D–deficient animals with electron microscopic procedures identified calcium lining the inside of the brush border plasma membrane, which left the microvillus following vitamin D or $1,25(OH)_2D$ administration [9–11]. Thus, the block in moving calcium through the intestinal epithelium is not simply that of getting calcium into the microvillus, but getting it out. Removing the microvillar calcium would then enable the Trpv6 channel to allow more calcium into the cell. Therefore, we considered the possibility that Myo1a, by moving CaM in and out of the microvillus with its bound calcium, could modulate these initial steps in calcium transport. The dynamic binding of Myo1a within the microvillus (80% turnover in 1 minute using FRAP measurements with Myo1a-GFP expressed in LLC-PK1-CL4 cells [26]) support this possibility.

We first developed full-length Myo1a sense and antisense constructs to determine whether we could enhance calcium transport by overexpressing Myo1a in C2Bbe cells or inhibit calcium transport by blocking Myo1a expression. The sense construct colocalized with actin in the brush border of these cells, as expected. The morphology of the cells was not affected by these manipulations (data not shown). As expected, $1,25(OH)_2D$ increased calcium transport by these cells in confirmation of the work from other laboratories [33],

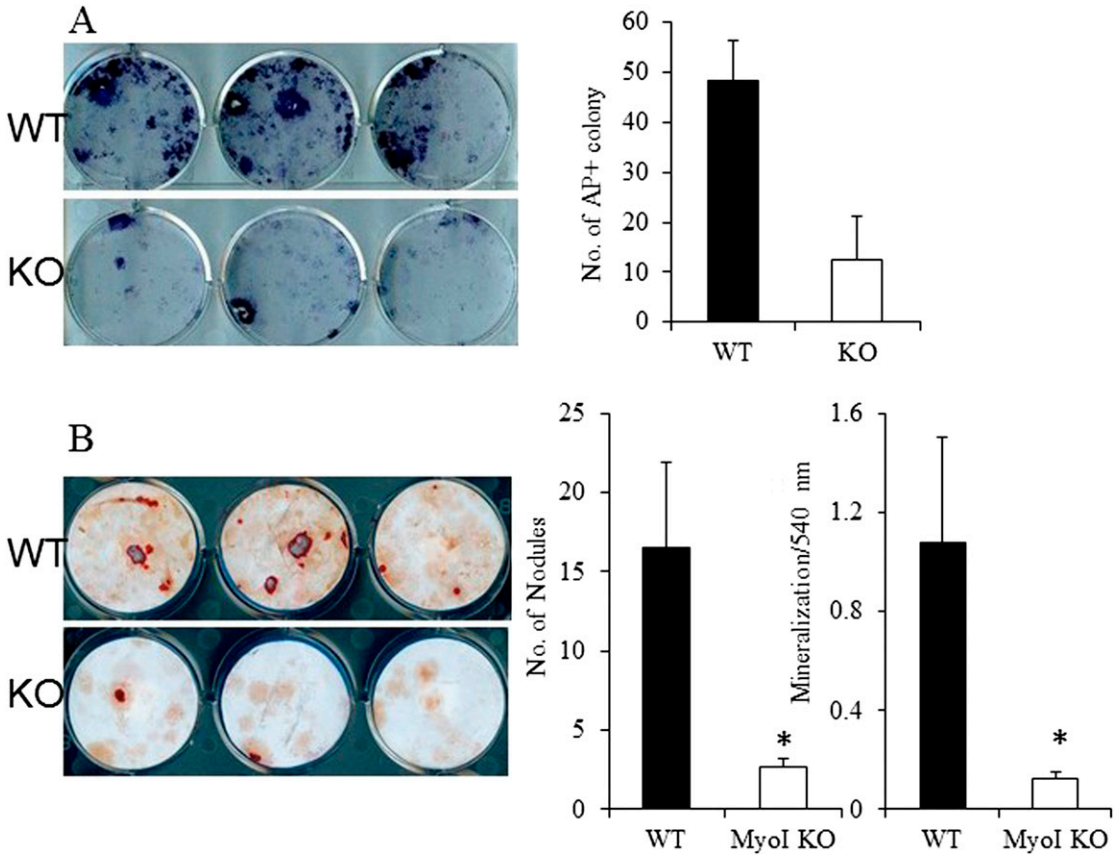

Figure 10. BMSCs from *Myo1a*-null mice show reduced differentiation *in vitro*. BMSCs were obtained from the femur and tibia of Myo1a-null and control mice (WT). On day 5, they were switched to differentiation media, following which AP- expressing colonies were quantitated on day 14 and Alizarin Red–stained mineralization nodules on day 21. As shown, the BMSCs from the Myo1a-null mice (KO) have a marked reduction in (A) AP-stained colonies and (B) mineralization nodule formation. The photos in A and B are representative pictures of the cultures. The bar graph in A showed number of AP-positive colonies/well in the WT and KO. The bar graphs in B showed number of mineralization nodules per well (left) and the spectrum analyzer readings from each well after eluting with 10% CPC (right). For all bar graphs, results are expressed as mean ± SD. Three wells for each mouse. n = 5 for WT; n = 4 for KO. *$P < 0.05$ KO (white bars) vs WT (black bars).

and this increase was accompanied by increased expression of Trpv6, also in confirmation of the work of others [1–4, 34]. Overexpression of Myo1a increased while inhibition of Myo1a expression blocked 1,25$(OH)_2$D-stimulated calcium transport. Basal levels of calcium transport were increased by overexpression of Myo1a, but inhibition of Myo1a expression did not alter basal levels. Moreover, Myo1a formed a complex with Trpv6 and CaM in these cells, supporting our hypothesis.

To test the role of Myo1a in intestinal calcium transport *in vivo* and its relationship with Trpv6, we examined calcium transport in mice null for either *Myo1a* or *Trpv6* or both. As expected and in confirmation of the work of some [28] but not all [29, 35] studies, the *Trpv6*-null mice showed a marked decrease in intestinal calcium transport compared with controls. Our results differed from those of others [28, 29, 35] in that the differences in calcium transport between null and control mice were more readily seen in mice ingesting 0.42% and 2.0% calcium diets than the 0.02% calcium diet, perhaps because we used a different technique (ligated loop vs everted loop or oral gavage) in which compensatory factors for the loss of Trpv6 were blunted by the higher calcium diet in this *in vivo* preparation measuring calcium transport from a defined section of the intestine than in other preparations that are *in vitro* or not limited to the

duodenum. This requires further investigation. More to the point of our hypothesis, the *Myo1a*-null mice failed to show a defect in intestinal calcium transport and failed to alter (synergize with) the reduced intestinal calcium transport in the *Trpv6*-null mice. This was surprising and inconsistent with the *in vitro* studies using a human intestinal cell line. Thus, at least in mice, Myo1a appears to have little impact on intestinal calcium transport. Understanding these apparent species differences remains a topic for future investigation.

Anticipating that alterations in intestinal calcium transport would result in changes in skeletal structure, we first performed μCT assessments of the tibiae of 3-month-old mice null for *Myo1a*, *Trpv6*, or both (similar results were seen at 6 months, data not shown). Based on the results with intestinal calcium transport and as previously reported [28, 36], we anticipated that the *Trpv6*-null mice would have a skeletal phenotype, but not the *Myo1a*-null mice, and that the double-null mice would resemble that of the *Trpv6*-null mice. To our great surprise, our expectations were 180° wrong. The *Trpv6*-null mice showed an increase in cancellous and cortical bone with increased trabecular thickness and connectivity density in the proximal tibia, although cortical thickness was not altered. This is not a result of loss of the Trpv6 in bone, as this protein is not expressed in bone to any extent, as we demonstrated in this study in confirmation of the findings of others [36], although other Trpv channels such as Trpv4 have been found in osteoblasts and influence calcium signaling in those cells [37]. Previous studies [36] with 2-month-old mice, presumably of the mixed B6/129 background, likewise failed to show a reduction in BV/TV in the null mice on a normal diet, although it was not increased, unlike our results. At this point, we have no clear explanation for the increased bone seen in our *Trpv6*-null mice, although the increased PTH and $1,25(OH)_2D$ found in other studies in these mice [28, 29] may be more anabolic than catabolic under the conditions of our experiments. This requires further investigation.

The greatest surprise was the profound decrease in bone in the *Myo1a*-null mice, a loss that dominated the anabolic changes found in the *Trpv6*-null mice when the double-null mice were examined. This could not be explained by changes in calcium absorption from the intestine, the only tissue previously known to express Myo1a. Exploring this unexpected result, we demonstrated expression of Myo1a in the osteoblasts and osteocytes and found that in its absence markers of osteoblast differentiation (OCN) were decreased. *In vitro*, BMSCs formed fewer osteoblast colonies capable of expressing AP or mineralizing. We cannot say at this point what role Myo1a is playing in osteoblasts. However, it is reasonable to anticipate that its ability to interact with actin as a CaM-dependent mechanoenzyme plays a role in its function in osteoblasts as it does in intestinal epithelial cells [38]. Transient dynamic actin cytoskeletal changes have been shown to stimulate osteoblast differentiation [39], a role that might require Myo1a. Similarly, calcium/CaM is well known to alter osteoblast proliferation and differentiation in part through the regulation of CaM kinase II and calcineurin [40, 41]. Myo1a could alter the distribution of calcium/CaM within the cell, thus serving to regulate access of these molecules to the enzymes regulating the differentiation process. These are exciting observations of a potential player in skeletal growth. However, future studies are required to elucidate this unexpected role of Myo1a in osteoblast differentiation and function.

Acknowledgments

We appreciate the gift of *Myo1a*-null mice from Dr. Mark Mooseker and the *Trpv6*-null mice from Dr. Matthias Hediger.

Financial Support: This work was supported by VA Merit Review Grant BX 003814 and National Institutes of Health Grants R01 055924, R01 DK28116, and R01 AR38386.

Additional Information

Correspondence: Daniel D. Bikle, MD, PhD, Department of Medicine and Endocrine Research Unit, Veterans Affairs Medical Center and University of California San Francisco, 1700 Owens St., San Francisco, California 94158. E-mail: daniel.bikle@ucsf.edu.

Disclosure Summary: The authors have nothing to disclose.

Data Availability: All data generated or analyzed during this study are included in this published article or in the data repositories listed in References.

References and Notes

1. Hoenderop JG, Nilius B, Bindels RJ. Calcium absorption across epithelia. *Physiol Rev*. 2005;**85**(1): 373–422.
2. Song Y, Peng X, Porta A, Takanaga H, Peng JB, Hediger MA, Fleet JC, Christakos S. Calcium transporter 1 and epithelial calcium channel messenger ribonucleic acid are differentially regulated by 1,25 dihydroxyvitamin D3 in the intestine and kidney of mice. *Endocrinology*. 2003;**144**(9):3885–3894.
3. Wood RJ, Tchack L, Taparia S. 1,25-Dihydroxyvitamin D3 increases the expression of the CaT1 epithelial calcium channel in the Caco-2 human intestinal cell line. *BMC Physiol*. 2001;**1**(1):11.
4. Bouillon R, Van Cromphaut S, Carmeliet G. Intestinal calcium absorption: molecular vitamin D mediated mechanisms. *J Cell Biochem*. 2003;**88**(2):332–339.
5. Bödding M. Voltage-dependent changes of TRPV6-mediated Ca2+ currents. *J Biol Chem*. 2005;**280**(8): 7022–7029.
6. den Dekker E, Hoenderop JG, Nilius B, Bindels RJ. The epithelial calcium channels, TRPV5 & TRPV6: from identification towards regulation. *Cell Calcium*. 2003;**33**(5-6):497–507.
7. Lambers TT, Weidema AF, Nilius B, Hoenderop JG, Bindels RJ. Regulation of the mouse epithelial Ca2(+) channel TRPV6 by the Ca(2+)-sensor calmodulin. *J Biol Chem*. 2004;**279**(28):28855–28861.
8. Hirnet D, Olausson J, Fecher-Trost C, Bödding M, Nastainczyk W, Wissenbach U, Flockerzi V, Freichel M. The TRPV6 gene, cDNA and protein. *Cell Calcium*. 2003;**33**(5-6):509–518.
9. Schäfer HJ. Ultrastructure and ion distribution of the intestinal cell during experimental vitamin-D deficiency rickets in rats. *Virchows Arch A Pathol Pathol Anat*. 1973;**359**(2):111–123.
10. Sampson HW, Matthews JL, Martin JH, Kunin AS. An electron microscopic localization of calcium in the small intestine of normal, rachitic, and vitamin-D-treated rats. *Calcif Tissue Res*. 1970;**5**(4): 305–316.
11. Chandra S, Fullmer CS, Smith CA, Wasserman RH, Morrison GH. Ion microscopic imaging of calcium transport in the intestinal tissue of vitamin D-deficient and vitamin D-replete chickens: a 44Ca stable isotope study. *Proc Natl Acad Sci USA*. 1990;**87**(15):5715–5719.
12. Bikle DD, Morrissey RL, Zolock DT. The mechanism of action of vitamin D in the intestine. *Am J Clin Nutr*. 1979;**32**(11):2322–2328.
13. Bikle DD, Zolock DT, Morrissey RL, Herman RH. Independence of 1,25-dihydroxyvitamin D3-mediated calcium transport from de novo RNA and protein synthesis. *J Biol Chem*. 1978;**253**(2):484–488.
14. Bikle DD, Munson S, Zolock DT. Calcium flux across chick duodenal brush border membrane vesicles: regulation by 1,25-dihydroxyvitamin D. *Endocrinology*. 1983;**113**(6):2072–2080.
15. Bikle DD, Munson S, Chafouleas J. Calmodulin may mediate 1,25-dihydroxyvitamin D-stimulated intestinal calcium transport. *FEBS Lett*. 1984;**174**(1):30–33.
16. Heintzelman MB, Mooseker MS. Assembly of the intestinal brush border cytoskeleton. *Curr Top Dev Biol*. 1992;**26**:93–122.
17. Bikle DD, Munson S. 1,25-Dihydroxyvitamin D increases calmodulin binding to specific proteins in the chick duodenal brush border membrane. *J Clin Invest*. 1985;**76**(6):2312–2316.
18. Swanljung-Collins H, Collins JH. Ca2+ stimulates the Mg2(+)-ATPase activity of brush border myosin I with three or four calmodulin light chains but inhibits with less than two bound. *J Biol Chem*. 1991; **266**(2):1312–1319.
19. Wang Y, Nishida S, Boudignon BM, Burghardt A, Elalieh HZ, Hamilton MM, Majumdar S, Halloran BP, Clemens TL, Bikle DD. IGF-I receptor is required for the anabolic actions of parathyroid hormone on bone. *J Bone Min Res*. 2007;**22**(9):1329–1337.
20. Bouxsein ML, Boyd SK, Christiansen BA, Guldberg RE, Jepsen KJ, Muller R. Guidelines for assessment of bone microstructure in rodents using micro-computed tomography. *J Bone Min Res*. 2010; **25**(7):1468–1486.
21. RRID:AB_2148170, http://antibodyregistry.org/search.php?q=AB_2148170.
22. RRID:AB_2810213, http://antibodyregistry.org/search?q=AB_2810213.
23. RRID:AB_2792976, http://antibodyregistry.org/search?q=AB_2792976.
24. RRID:AB_2810256, http://antibodyregistry.org/search?q=2810256.
25. RRID:AB_2069454, http://antibodyregistry.org/search?q=AB_2069454.
26. Tyska MJ, Mooseker MS. MYO1A (brush border myosin I) dynamics in the brush border of LLC-PK1-CL4 cells. *Biophys J*. 2002;**82**(4):1869–1883.

27. Wang Y, Sakata T, Elalieh HZ, Munson SJ, Burghardt A, Majumdar S, Halloran BP, Bikle DD. Gender differences in the response of CD-1 mouse bone to parathyroid hormone: potential role of IGF-I. *J Endocrinol*. 2006;**189**(2):279–287.
28. Bianco SD, Peng JB, Takanaga H, Suzuki Y, Crescenzi A, Kos CH, Zhuang L, Freeman MR, Gouveia CH, Wu J, Luo H, Mauro T, Brown EM, Hediger MA. Marked disturbance of calcium homeostasis in mice with targeted disruption of the Trpv6 calcium channel gene. *J Bone Min Res*. 2007;**22**(2):274–285.
29. Benn BS, Ajibade D, Porta A, Dhawan P, Hediger M, Peng JB, Jiang Y, Oh GT, Jeung EB, Lieben L, Bouillon R, Carmeliet G, Christakos S. Active intestinal calcium transport in the absence of transient receptor potential vanilloid type 6 and calbindin-D9k. *Endocrinology*. 2008;**149**(6):3196–3205.
30. Peng JB, Chen XZ, Berger UV, Vassilev PM, Tsukaguchi H, Brown EM, Hediger MA. Molecular cloning and characterization of a channel-like transporter mediating intestinal calcium absorption. *J Biol Chem*. 1999;**274**(32):22739–22746.
31. Zhuang L, Peng JB, Tou L, Takanaga H, Adam RM, Hediger MA, Freeman MR. Calcium-selective ion channel, CaT1, is apically localized in gastrointestinal tract epithelia and is aberrantly expressed in human malignancies. *Lab Invest*. 2002;**82**(12):1755–1764.
32. Bikle DD, Munson S. The villus gradient of brush border membrane calmodulin and the calcium-independent calmodulin-binding protein parallels that of calcium-accumulating ability. *Endocrinology*. 1986;**118**(2):727–732.
33. Fleet JC, Wood RJ. Specific 1,25(OH)2D3-mediated regulation of transcellular calcium transport in Caco-2 cells. *Am J Physiol*. 1999;**276**(4):G958–G964.
34. van Abel M, Hoenderop JG, van der Kemp AW, van Leeuwen JP, Bindels RJ. Regulation of the epithelial Ca2+ channels in small intestine as studied by quantitative mRNA detection. *Am J Physiol Gastrointest Liver Physiol*. 2003;**285**(1):G78–G85.
35. Kutuzova GD, Sundersingh F, Vaughan J, Tadi BP, Ansay SE, Christakos S, Deluca HF. TRPV6 is not required for 1alpha,25-dihydroxyvitamin D3-induced intestinal calcium absorption in vivo. *Proc Natl Acad Sci USA*. 2008;**105**(50):19655–19659.
36. Lieben L, Benn BS, Ajibade D, Stockmans I, Moermans K, Hediger MA, Peng JB, Christakos S, Bouillon R, Carmeliet G. Trpv6 mediates intestinal calcium absorption during calcium restriction and contributes to bone homeostasis. *Bone*. 2010;**47**(2):301–308.
37. Son A, Kang N, Kang JY, Kim KW, Yang YM, Shin DM. TRPM3/TRPV4 regulates Ca2+-mediated RANKL/NFATc1 expression in osteoblasts. *J Mol Endocrinol*. 2018;**61**(4):207–218.
38. Tyska MJ, Mackey AT, Huang JD, Copeland NG, Jenkins NA, Mooseker MS. Myosin-1a is critical for normal brush border structure and composition. *Mol Biol Cell*. 2005;**16**(5):2443–2457.
39. Wu XT, Sun LW, Qi HY, Shi H, Fan YB. The bio-response of osteocytes and its regulation on osteoblasts under vibration. *Cell Biol Int*. 2016;**40**(4):397–406.
40. Yu L, Ma X, Sun J, Tong J, Shi L, Sun L, Zhang J. Fluid shear stress induces osteoblast differentiation and arrests the cell cycle at the G0 phase via the ERK1/2 pathway. *Mol Med Rep*. 2017;**16**(6): 8699–8708.
41. Zayzafoon M. Calcium/calmodulin signaling controls osteoblast growth and differentiation. *J Cell Biochem*. 2006;**97**(1):56–70.